Extended X-Ray Absorption Fine Structure, Crystal Structures at 295 and 173 K, and Electron Paramagnetic Resonance and Electronic Spectra of Bis[tris(2-pyridyl)-methane]copper(II) Dinitrate†

Timothy Astley,[a] Paul J. Ellis,[b] Hans C. Freeman,*[,b] Michael A. Hitchman,*[,a] F. Richard Keene[c] and Edward R. T. Tiekink[d]

[a] *Chemistry Department, University of Tasmania, Box 252C, Hobart, Tasmania 7000, Australia*
[b] *Department of Inorganic Chemistry, University of Sydney, NSW 2006, Australia*
[c] *Department of Molecular Sciences, James Cook University of North Queensland, Townsville, Queensland 4811, Australia*
[d] *Department of Chemistry, The University of Adelaide, Adelaide, South Australia 5005, Australia*

The crystal structure of bis[tris(2-pyridyl)methane]copper(II) dinitrate, $[Cu\{(C_5H_4N)_3CH\}_2][NO_3]_2$ has been determined. At 295 K the Cu atom lies on a special position so that all six Cu–N bonds are crystallographically equivalent [Cu–N 2.103(4) Å]. The structure at 173 K is very similar [Cu–N 2.095(3) Å]. However, the electronic spectrum suggests that the Cu^{2+} ion experiences a ligand field of tetragonal symmetry. This has been confirmed by the EXAFS of the compound, which shows four nitrogen atoms at 2.04 Å and two at 2.25 Å from the copper. The apparent trigonal symmetry revealed by the X-ray analysis is thus due to disorder of the long and short Cu–N bonds about the three-fold axis. The EPR spectrum shows an isotropic signal at 295 K, but a signal characteristic of a tetragonally elongated octahedral complex at 150 K. This suggests that the directions of the long and short bonds interchange rapidly on the EPR time-scale at room temperature, but that the complexes become frozen into particular orientations on cooling.

Tripodal ligands involving nitrogen-donor heterocycles have been found to exhibit a number of useful properties in co-ordination and organometallic chemistry.[1] As part of a study of the electronic and steric characteristics of transition-metal complexes of ligands of this kind,[2–7] we have prepared the compound $[Cu\{(C_5H_4N)_3CH\}_2][NO_3]_2$, where $(C_5H_4N)_3CH$ is tris(2-pyridyl)methane. We report here the crystal structures of the compound at 295 and 173 K. These are closely similar. In both structures the metal and bridgehead carbon atoms of the $[Cu\{(C_5H_4N)_3CH\}_2]^{2+}$ complex lie on a three-fold symmetry axis, so that the six Cu–N bonds are crystallographically equivalent. Six equivalent bonds in such a complex would be highly unusual, as they would lead to an orbitally degenerate ground state, which is unstable with respect to a Jahn–Teller distortion. The electronic spectrum of the compound is also reported, and is closely similar to those of analogous complexes which have the tetragonally distorted octahedral co-ordination geometry commonly observed for Cu^{II}.[6,7] This suggests that the *local* co-ordination geometry may be a tetragonally distorted octahedron, and that the crystallographic symmetry results from disorder of the Cu–N bonds about the three-fold axis. Disorder of this kind has been observed for other Cu^{II} compounds, such as $[Cu(en)_3]SO_4$ (en = ethane-1,2-diamine).[8] The disorder model for $[Cu\{(C_5H_4N)_3CH\}_2][NO_3]_2$ is supported by the electron paramagnetic resonance (EPR) spectrum which shows an isotropic signal at 293 K but a signal characteristic of a tetragonally elongated octahedral complex at 150 K.

† *Supplementary data available:* (SUP No. 57060, 7 pp.). Observed EXAFS data, final positional parameters and Debye–Waller factors. See Instructions for Authors, *J. Chem. Soc., Dalton Trans.*, 1995, Issue 1, pp. xxv–xxx.

Non-SI units employed: eV ≈ 1.60 × 10^{-19} J, G = 10^{-4} T.

As an additional probe of the Cu^{II} stereochemistry in $[Cu\{(C_5H_4N)_3CH\}_2][NO_3]_2$ we have measured the extended X-ray absorption fine structure (EXAFS) of the compound. This is dominated by contributions from back-scattering atoms in the immediate vicinity of an X-ray absorber (in the present case, the Cu atom). In solids where the apparent structure revealed by X-ray diffraction may be affected by disorder, EXAFS provides a powerful means of studying the local co-ordination geometry. For example, we have recently used the EXAFS of the 3-chloroanilinium salt $[NH_3C_6H_4Cl\text{-}3]_8[CuCl_6]Cl_4$ to confirm that the tetragonally compressed geometry of the $[CuCl_6]^{4-}$ complex derived from an X-ray crystal-structure analysis[9] was in fact due to a superposition of disordered $[CuCl_6]^{4-}$ ions having the normal elongated tetragonal geometry.[10] The EXAFS data for $[Cu\{(C_5H_4N)_3CH\}_2][NO_3]_2$ likewise show that the local geometry around the Cu atom is elongated tetragonal, the Cu–N distances being in good agreement with the electronic and EPR spectra.

Experimental

Synthesis of $[Cu\{(C_5H_4N)_3CH\}_2][NO_3]_2$.—A solution of tris(2-pyridyl)methane[4] (80 mg, 0.323 mmol) in acetone (10 cm^3) was added dropwise with stirring to a solution of $Cu(NO_3)_2{\cdot}3H_2O$ (35 mg, 0.145 mmol) in the same solvent (15 cm^3). The mixture was cooled and the light blue product separated by centrifugation. Yield 86 mg, 87%. The solid was recrystallised from methanol–diethyl ether (Found: C, 56.4; H, 3.85; N, 16.4. Calc. for $C_{32}H_{26}CuN_8O_6$: C, 56.3; H, 3.85; N, 16.4%). Crystals suitable for diffraction measurements were obtained by evaporation of an ethanolic solution.

Spectroscopic Measurements.—Single-crystal electronic spectra were measured using a Cary 5A spectrophotometer. The procedure is described elsewhere.[11] The sample was cooled

Table 1 Crystal data for $[Cu\{(C_5H_4N)_3CH\}_2][NO_3]_2$*

	295 K	173 K
a/Å	11.677(3)	11.607(3)
c/Å	17.999(4)	17.906(6)
U/Å^3	2125.7(9)	2089(1)
D_c/g cm^{-3}	1.599	1.626
μ/cm^{-1}	8.35	8.49
Max., min. transmission factors	1.081, 0.794	1.084, 0.826
No. data measured	1247	1245
No. unique data	653	645
No. observed data [$I \geqslant 2.5\sigma(I)$]	496	556
R	0.046	0.035
R'	0.048	0.045

* Details in common: formula $C_{32}H_{26}CuN_8O_6$, M 682.2, space group $R\bar{3}$, $Z = 3$, $F(000)$ 1053; $w = 1/\sigma^2(F)$.

Table 2 Fractional atomic coordinates for the non-hydrogen atoms of $[Cu\{(C_5H_4N)_3CH\}_2][NO_3]_2$

Atom	x	y	z
295 K			
Cu[a]	1.0	0.0	1.0
O(1)	0.6667(5)	0.2275(5)	0.9787(3)
N(1)[b]	$\frac{2}{3}$	$\frac{1}{3}$	0.9705(6)
N(11)	0.9861(5)	0.1349(5)	0.9285(2)
C(1)[b]	1.0	0.0	0.8305(4)
C(12)	0.9701(6)	0.2320(7)	0.9523(3)
C(13)	0.9589(6)	0.3177(7)	0.9050(4)
C(14)	0.9648(6)	0.3015(6)	0.8288(4)
C(15)	0.9820(6)	0.2010(6)	0.8038(3)
C(16)	0.9897(5)	0.1168(5)	0.8549(3)
173 K			
Cu[a]	1.0	0	1.0
O(1)	0.5595(3)	0.2270(3)	0.9778(2)
N(1)[b]	$\frac{2}{3}$	$\frac{1}{3}$	0.9736(3)
N(11)	0.9867(3)	−0.1481(3)	0.9277(1)
C(1)[b]	1.0	0	0.8289(3)
C(12)	0.9723(4)	−0.2646(4)	0.9510(2)
C(13)	0.9601(4)	−0.3607(4)	0.9045(2)
C(14)	0.9658(4)	−0.3388(4)	0.8287(2)
C(15)	0.9828(4)	−0.2190(3)	0.8029(2)
C(16)	0.9912(3)	−0.1280(3)	0.8542(2)

[a] Atom has $\frac{1}{6}$ site occupancy factor. [b] Atom has $\frac{1}{3}$ site occupancy factor.

using a Cryodyne model 22C cryostat. The reflectance spectrum was recorded with a Beckmann DK2A spectrophotometer. The EPR spectra were measured at Q-band frequency, ≈34 GHz, using a JEOL JES-FE spectrometer equipped with a standard JEOL cryostat and temperature controller.

Crystallography.—Intensity data were measured on a Rigaku AFC6R diffractometer fitted with a graphite monochromator [λ(Mo-Kα) = 0.710 73 Å, ω–2θ mode, θ_{max} = 27.5°]. A single crystal (0.13 × 0.18 × 0.24 mm) was used to record data at 295 and 173 K. No decomposition of the crystal occurred during the data collections. Absorption corrections were applied.[12] Reflections with $I \geqslant 3.0\sigma(I)$ were used in the analyses. Crystal data are summarized in Table 1.

The structure was solved by conventional heavy-atom methods and refined by a full-matrix least-squares procedure based on F.[13] Non-hydrogen atoms were refined with anisotropic thermal parameters. Hydrogen atoms were located in a difference map during the 295 K analysis. They were included in the model at their calculated positions (C–H 0.97 Å) and were assigned plausible isotropic thermal parameters. At convergence (sigma weights) R = 0.046 and R' = 0.048 for the 295 K data, and R = 0.035 and R' = 0.045 for the 173 K data. The analysis of variance showed no special features. The highest peak in the final difference map was 0.50 e Å^{-3} for the 295 K data and 0.38 e Å^{-3} for the 173 K data. Scattering factors for all atoms were those incorporated in the TEXSAN program.[13]

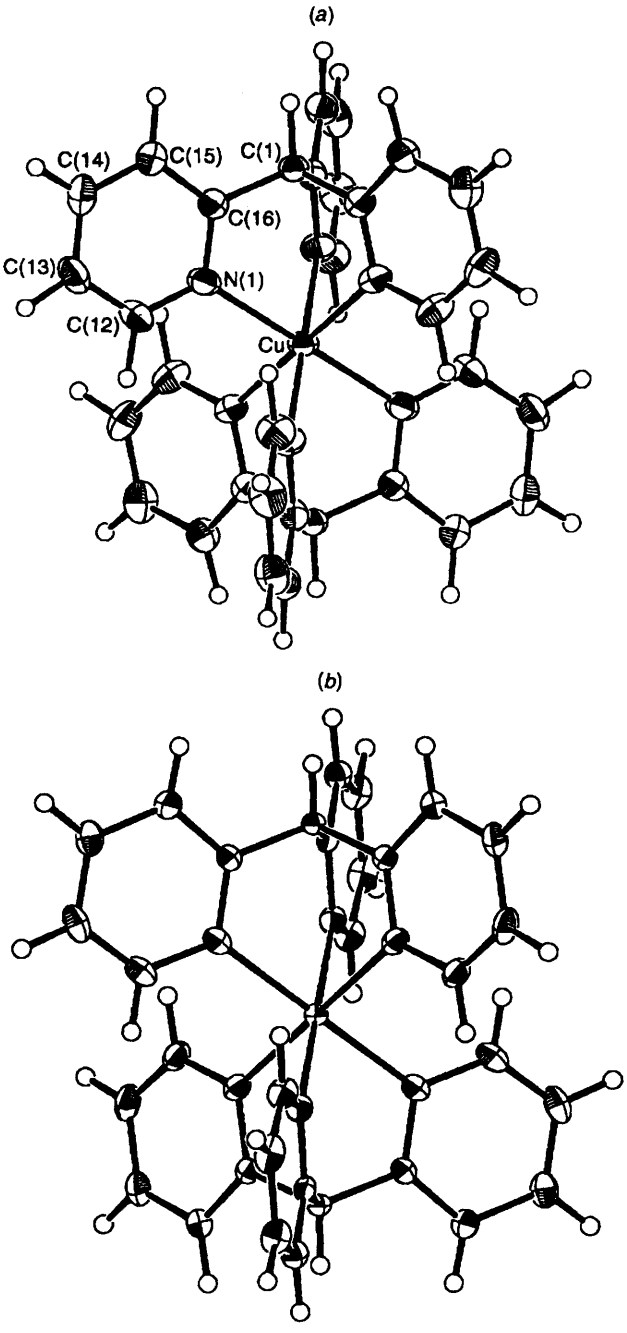

Fig. 1 Molecular structure (ORTEP[14]) and atom labelling for the $[Cu\{(C_5H_4N)_3CH\}_2]^{2+}$ complex in $[Cu\{(C_5H_4N)_3CH\}_2][NO_3]_2$ at (*a*) 295 K and (*b*) 173 K. The thermal ellipsoids are drawn at the 35% probability level

The structure and atom labelling scheme are shown in Fig. 1. The fractional atomic coordinates of the non-hydrogen atoms are listed in Table 2, bond distances and angles in Table 3 and anisotropic thermal ellipsoid parameters in Table 4.

Additional material available from the Cambridge Crystallographic Data Centre comprises H-atom coordinates and remaining bond lengths and angles.

EXAFS.—X-Ray absorption measurements were made at the Australian National Beamline Facility on bending-magnet beamline 20B at the KEK Photon Factory, Tsukuba, Japan. The storage ring delivered a current of 330–300 mA at 2.5 GeV. The monochromator was a Si(111) channel-cut double crystal.

No detuning was applied. The X-ray spectra were recorded in transmission mode using standard N_2-filled ionisation chambers. Energies were calibrated by means of a Cu-foil internal standard, the first inflection point on the Cu edge being assigned as 8980.3 eV.

The sample of $[Cu\{(C_5H_4N)_3CH\}_2][NO_3]_2$ was a finely ground powder diluted with BN (boron nitride). The mixture was pressed into a pellet (1 mm thick) supported in an Al spacer with 63.5 μm Mylar tape windows. Two scans of the X-ray absorption spectrum were recorded at ambient temperature (295 K). The scans were averaged using weights based on the signal-to-noise ratios. A background correction was applied by fitting a polynomial to the pre-edge region, extrapolating it into the EXAFS region and subtracting it from the data. A three-region spline was fitted to the EXAFS region and subtracted. The data were normalised to an edge jump of 1.0 and compensated for decreasing absorbance past the edge. The background-subtracted, normalised and compensated data were converted to k space, where k is the photoelectron wavevector $\hbar^{-1}[2m_e(E - E_0)]^{\frac{1}{2}}$ and E_0 is the threshold energy.

For the EXAFS refinement of the structure, a model comprising the non-H atoms of the $(C_5H_4N)_3CH$ ligand was constructed using the known geometry of the $(C_5H_4N)CH$ fragment in $[Cu\{(pz)_2(C_5H_4N)CH\}_2]^{2+}$ (pz = pyrazol-1-yl).[6] The geometry of the model is shown in Fig. 2. The three Cu–N(pyridyl) bonds were initially assigned lengths 2.0, 2.1 and 2.3 Å. The single-scattering Debye–Waller factors, $2\sigma^2$, were assigned typical room-temperature values [0.01 $Å^2$ for the N(pyridyl) atoms, increasing to 0.02 $Å^2$ for the most distant atoms]. In keeping with the stoichiometry of the complex, the atoms of the ligand molecule were given multiplicity 2.

In the refinement calculations (see below), the positions and Debye–Waller factors of all atoms in the model were treated as variables. The number of *independent* variables was, however,

Table 3 Selected bond distances (Å) and angles (°) for $[Cu\{(C_5H_4N)_3CH\}_2][NO_3]_2$

	295 K	173 K
Cu–N(11)	2.103(4)	2.095(3)
N(11)–C(12)	1.310(7)	1.343(4)
N(11)–C(16)	1.345(6)	1.334(4)
C(1)–C(16)	1.494(6)	1.506(4)
C(12)–C(13)	1.370(9)	1.340(5)
C(13)–C(14)	1.391(9)	1.377(6)
C(14)–C(15)	1.362(8)	1.382(5)
C(15)–C(16)	1.381(7)	1.367(4)
N(1)–O(1)	1.245(5)	1.242(3)
N(11)–Cu–N(11^{i})	93.6(2)	94.1(1)
N(11)–Cu–N(11^{ii})	86.4(2)	85.9(1)
Cu–N(11)–C(12)	123.1(4)	123.8(2)
Cu–N(11)–C(16)	117.7(4)	119.0(2)
C(12)–N(11)–C(16)	119.2(5)	117.2(3)
C(16)–C(1)–C(16^{ii})	111.7(3)	111.4(2)
N(11)–C(12)–C(13)	122.4(5)	123.6(3)
C(12)–C(13)–C(14)	118.9(6)	118.9(3)
C(13)–C(14)–C(15)	118.8(6)	119.1(4)
C(14)–C(15)–C(16)	118.9(5)	118.1(4)
N(11)–C(16)–C(1)	117.1(5)	116.6(3)
N(11)–C(16)–C(15)	121.7(5)	123.1(3)
C(1)–C(16)–C(15)	121.2(5)	120.2(3)
O(1)–N(1)–O(1^{iii})	119.2(5)	119.64(7)

Symmetry operations: i, $x - y, x - 1, 2 - z$; ii, $1 - y, x - y - 1, z$; iii, $1 - y, x - y, z$.

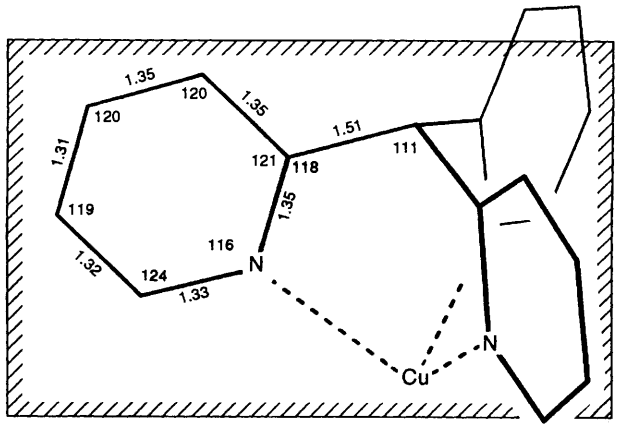

Fig. 2 Ideal EXAFS model geometry. The mirror plane is represented by the shaded rectangle

Table 4 Anisotropic thermal parameters ($Å^2$) for $[Cu\{(C_5H_4N)_3CH\}_2][NO_3]_2$

Atom	U_{11}	U_{22}	U_{33}	U_{12}	U_{13}	U_{23}
295 K						
Cu	0.0389(6)	0.0389(6)	0.0266(7)	0.0194(7)	0	0
O(1)	0.092(4)	0.071(4)	0.117(4)	0.043(4)	0.005(3)	−0.004(4)
N(1)	0.069(5)	0.069(5)	0.076(8)	0.035(8)	0	0
N(11)	0.049(3)	0.047(3)	0.034(2)	0.026(3)	0.001(2)	−0.005(2)
C(1)	0.037(3)	0.037(3)	0.028(5)	0.018(5)	0	0
C(12)	0.066(5)	0.049(4)	0.048(4)	0.031(4)	0.005(3)	−0.012(3)
C(13)	0.060(5)	0.045(4)	0.069(5)	0.029(4)	0.010(4)	−0.012(4)
C(14)	0.052(4)	0.035(4)	0.074(4)	0.021(3)	0.004(4)	0.006(4)
C(15)	0.045(4)	0.040(3)	0.047(3)	0.021(3)	−0.001(3)	0.003(3)
C(16)	0.033(3)	0.035(3)	0.040(3)	0.014(3)	0.001(3)	−0.003(3)
173 K						
Cu	0.0210(3)	0.0210(3)	0.0180(4)	0.0105(4)	0	0
O(1)	0.042(2)	0.057(2)	0.057(2)	0.027(2)	0.003(1)	0.001(2)
N(1)	0.040(2)	0.040(2)	0.039(3)	0.020(3)	0	0
N(11)	0.026(2)	0.029(2)	0.028(1)	0.013(1)	0.001(1)	0.006(1)
C(1)	0.022(2)	0.022(2)	0.018(2)	0.011(2)	0	0
C(12)	0.033(2)	0.037(2)	0.035(2)	0.021(2)	0.003(2)	0.012(2)
C(13)	0.033(2)	0.028(2)	0.054(2)	0.019(2)	0.006(2)	0.013(2)
C(14)	0.033(2)	0.029(2)	0.047(2)	0.020(2)	0.005(2)	0.001(2)
C(15)	0.027(2)	0.029(2)	0.031(2)	0.016(2)	0.001(2)	−0.001(2)
C(16)	0.018(2)	0.023(2)	0.025(2)	0.009(1)	0.002(1)	0.003(1)

The anisotropic thermal parameter is given by the expression: $T_{aniso} = \exp[-2\pi^2(h^2a^{*2}U_{11} + k^2b^{*2}U_{22} + l^2c^{*2}U_{33} + 2hka^*b^*U_{12} + 2hla^*c^*U_{13} + 2klb^*c^*U_{23})]$.

Table 5 Restraints and constraints used in the refinement of the $[Cu\{(C_5H_4N)_3CH\}_2][NO_3]_2$ model *versus* the observed EXAFS

	Ideal value/Å		Ideal value/Å
N(1)–C(16)	1.350	C(12)–N(1)–C(16)	116.0
N(1)–C(12)	1.330	N(1)–C(16)–C(15)	120.9
C(16)–C(15)	1.354	C(16)–C(15)–C(14)	119.5
C(12)–C(13)	1.323	C(15)–C(14)–C(13)	120.1
C(15)–C(14)	1.348	C(14)–C(13)–C(12)	119.1
C(13)–C(14)	1.308	C(13)–C(12)–N(1)	124.4
C(16)–C(1)	1.507	N(1)–C(16)–C(1)	117.6
		C(16)–C(1)–C(16)*	111.3

Debye–Waller factor restraints	Debye–Waller factor constraints
$\sigma^2_{C(16)} > \sigma^2_{N(1)}$	$\sigma^2_{C(13)} = \sigma^2_{C(14)} = \sigma^2_{C(15)}$
$\sigma^2_{C(12)} > \sigma^2_{N(1)}$	$\sigma^2_{C(13)} - \sigma^2_{C(12)} = \sigma^2_{C(13')} - \sigma^2_{C(12')}$
$\sigma^2_{C(15)} > \sigma^2_{C(16)}$	$\sigma^2_{C(13)} - \sigma^2_{N(1)} = \sigma^2_{C(12')} - \sigma^2_{N(1')}$
$\sigma^2_{C(13)} > \sigma^2_{C(12)}$	$\sigma^2_{C(16)} - \sigma^2_{N(1)} = \sigma^2_{C(16')} - \sigma^2_{N(1')}$

The same restraints are used for each of the three rings. The atoms of the ring lying on the mirror plane are indicated by primes. The σ values used in the refinement were 0.1 Å for all distance restraints, 5° for all angle restraints, and 0.002 Å² for all Debye–Waller factor restraints.

* This angle is the bond angle at the methyl carbon.

substantially reduced by applying appropriate restraints and constraints (Table 5). The bond lengths and bond angles were tightly restrained to the ideal geometry of Fig. 2. Additional restraints were applied to preserve the planarity of the pyridyl rings, to keep the Cu atom coplanar with each of the pyridyl rings, and to ensure that the single-scattering Debye–Waller factors of the ring atoms increased with increasing distance from the Cu atom. Constraints were applied to keep the Debye–Waller factors of the three atoms furthest from the Cu in each ring equal, and to make the increments between the Debye–Waller factors around the ring identical in all three rings. During the initial refinement cycles it was observed that the two shorter Cu–N(pyridyl) distances had refined to the same value. A plane of symmetry was accordingly introduced between these two pyridyl rings, resulting in a further reduction of the number of independent variables.

The EXAFS analysis was performed by means of the program XFIT[15] which uses non-linear least-squares fitting to vary the model until the agreement between the observed and calculated EXAFS is optimised. The EXAFS of the model was calculated *ab initio* using the curved-wave multiple-scattering EXAFS program FEFF 6.01.[16] The calculation included 151 unique paths with effective length < 5 Å and up to 6 legs. The Debye–Waller factors for the multiple-scattering paths were estimated from the single-scattering Debye–Waller factors using an uncorrelated isotropic vibration model.[15]

The quantity minimised during the refinements is given by equation (1), where $\chi_{calc}(k)$ and $\chi_{obs}(k)$ are the k^3-weighted and

$$X^2 = \int_{k=0}^{\infty} [\chi_{calc}(k) - \chi_{obs}(k)]^2 \, dk + \sum_i w_i \Delta_i^2 \quad (1)$$

Fourier-filtered values of the calculated and observed EXAFS, respectively. The k^3 weighting was applied to each EXAFS curve prior to Fourier filtering; Δ_i is the difference between the model parameter and the value to which it is restrained in the ith restraint, and w_i is the weight of the restraint; $w_i = \sigma_i^{-2}$ where σ_i is an arbitrary variance-like parameter.

The parameters varied were the position (x, y, z) and single-scattering Debye–Waller factor $2\sigma^2$ of each atom, the threshold energy E_0 and the scale factor ${S_0}^2$. The goodness-of-fit parameter R was calculated from equation (2). The standard

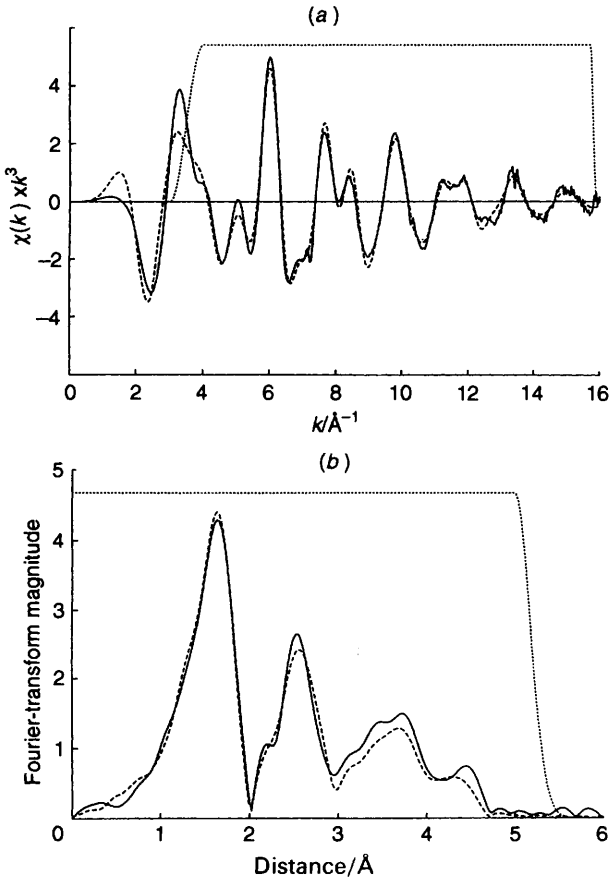

Fig. 3 (*a*) EXAFS of $[Cu\{(C_5H_4N)_3CH\}_2]^{2+}$: observed (——), calculated from refined model (- - - -), window used in Fourier filter (• • • •). (*b*) Fourier-transform amplitude of EXAFS: observed (——), calculated (- - - -), window used in Fourier filter (• • • •)

$$R = \int_{k=0}^{\infty} [\chi_{calc}(k) - \chi_{obs}(k)]^2 \, dk / \int_{k=0}^{\infty} \chi_{obs}(k)^2 \, dk \quad (2)$$

deviations were estimated by fitting the model to a number of EXAFS curves generated by first using a Fourier filter to smooth the observed EXAFS, and then adding random noise at the level found in the original observed EXAFS. The noise in the observed EXAFS was estimated using Fourier filtering.[15] The deviations obtained using this Monte-Carlo method were less than 0.002 Å for the Cu–N distances and 0.0005 Å² for the Cu–N Debye–Waller factors. These values represent solely the errors due to counting statistics. The fact that the values are small reflects the high quality of the EXAFS data. The systematic errors in the short and long Cu–N distances are typically estimated as *ca.* 0.01 and 0.02 Å, respectively, and these values are used in the text.

The observed and calculated EXAFS, the corresponding Fourier transforms, and the window functions used in the Fourier filter are shown in Fig. 3. The final R value was 0.168. The maximum deviation from ideal geometry was less than 0.01 Å for the bond lengths and 0.5° for the bond angles. The R value obtained by refining a model with the three-fold symmetry found in the X-ray diffraction analysis was 0.218. The Cu–N distance in the refined model with three-fold symmetry was 2.03 Å and the ${S_0}^2$ factor was low, indicating that the strong EXAFS from the two pyridine rings closer to the Cu atom had dominated the refinement. The refined Cu–N bond lengths and the first and second shell thermal parameters are shown in Table 6. The observed EXAFS data, and the final positional parameters and Debye–Waller factors for all atoms, have been deposited as SUP 57060.

Table 6 EXAFS analysis of $[Cu\{(C_5H_4N)_3CH\}_2][NO_3]_2$ at 295 K: main distances around Cu *

E_o/eV	8992.97(12)	
S_0^2	1.190(10)	
R factor	0.168 3	
Shell	Distance/Å	$2\sigma^2$/Å^2
4N	2.038 5(5)	0.012 87(12)
2N	2.250 3(15)	0.023 6(5)

* Standard deviations are given in parentheses. The estimated *systematic* errors in the distances for the two shells are 0.01–0.02 Å.

Results and Discussion

Crystal Structure.—The dimensions of the complex (Table 3) provide little reason to suspect that they represent anything other than the true geometry. The dimensions of the pyridyl rings are similar to those of the pyridyl rings in complexes of the related ligand $(pz)_2(C_5H_4N)CH$ (pz = pyrazol-1-yl).[6] The six crystallographically equivalent Cu–N(pyridyl) bonds have precisely the length, 2.10 Å, that would be predicted from the average of the M–N(pyridyl) bond lengths in $[M\{(pz)_2(C_5H_4N)CH\}_2][NO_3]_2$, M = Ni^{II} or Zn^{II}, at 295 K.[6] The only results that might be symptomatic of an underlying problem in the crystallographic refinements are that several of the ligand dimensions in Table 3 appear to undergo highly significant changes ($\geqslant 3\sigma$) between 295 and 173 K, and that these changes do not seem to be correlated with one another or with other features of the structure. A facile explanation of these observations is that the estimated standard deviations of the atomic positional coordinates are too low, but this merely emphasises that the refinements may not have converged to the optimum solution.

A more serious problem is that Cu^{II} complexes almost never have six identical copper–ligand bond lengths but adopt an elongated tetragonal co-ordination geometry. For example, in the centrosymmetric complex $[Cu\{(pz)_2(C_5H_4N)CH\}_2][NO_3]_2$ formed by another tripod ligand, the copper–ligand bond lengths are Cu–N(pyridyl) 2.020(3), Cu–N(pz) 1.994(3) and Cu–N(pz) 2.385(3) Å.[6] This lowering in symmetry is explained conventionally in terms of vibronic Jahn–Teller coupling, which acts to remove the orbital degeneracy that would occur in a regular octahedral Cu^{II} complex. It should be noted that a moderate distortion of the three symmetry related N–Cu–N angles from 90° (such as ≈86° in the present complex) does *not* suffice to remove the degeneracy. These effects are the subject of a recent review.[17]

Other examples of Cu^{II} complexes that crystallise with the metal atom on a three-fold symmetry axis and with six crystallographically equivalent metal–ligand bonds have been reported.[18] Detailed analysis has in each case revealed that four short and two long bonds occur at the *local* level, the high crystallographic symmetry being due to disorder of the bonds about the three-fold axis.[19] Clues are frequently (but not always) to be found in the crystallographically determined vibrational ellipsoids. For example, in the crystal structure of $[Cu(en)_3]SO_4$ (en = ethane-1,2-diamine), the elongation of the vibrational ellipsoids along the Cu–N bond vectors was taken as evidence of disorder in the positions of the nitrogen atoms.[8] In several instances, quantitative analysis of the vibrational parameters has yielded estimates of the local Cu^{II} co-ordination geometry.[19,20] On the other hand, in a study of the compound $[Cu(C_6H_5N_3)_2][Cu(CN)_3]\cdot 2H_2O$, an analysis of the crystallographic vibrational parameters failed to detect any disorder of the ligands, although this was clearly indicated by spectroscopic data.[21]

In the case of the present complex $[Cu\{(C_5H_4N)_3CH\}_2][NO_3]_2$, the vibrational parameters of the nitrogen atoms provide no evidence for disorder. The diagonalised vibration ellipsoid parameters (Table 4) and the vibrational ellipsoids derived from them (Fig. 1) both show that the deviations from spherical symmetry are not much larger for the nitrogen atoms than for the central Cu. Even at 173 K, where the decrease in vibrational amplitudes should make any effects due to disorder more apparent, the relative elongation of the ellipsoids is at best marginal (Fig. 1). The failure of the crystallographically derived vibrational ellipsoids to give any indication of disorder is puzzling, since the evidence for disorder from the EXAFS and electronic and EPR spectra of the compound is unequivocal (see later). An explanation that would be consistent with our earlier comments on the crystallographic refinement is that the disorder extends over a sufficiently large proportion of the atoms of the ligand to let the effects become lost in the noise of the experiment or 'averaged out'.

EXAFS.—The observed EXAFS is incompatible with the EXAFS calculated for a model with six equivalent pyridines, but is well matched by the EXAFS calculated after refinement of the model with four short and two long Cu–N bonds. The weighted average of the four shorter Cu–N distances, 2.04(±0.01) Å, and the two longer ones, 2.25(±0.02) Å, is 2.11(±0.01) Å, in good agreement with the crystallographic values, 2.103(4) Å at 295 K and 2.095(3) Å at 173 K.

Electronic Spectra.—At room temperature (298 K) the electronic reflectance spectrum of $[Cu\{(C_5H_4N)_3CH\}_2][NO_3]_2$ over the range 4000–22 000 cm^{-1} shows a band centred at ≈7000 cm^{-1} and a peak at 16 000 cm^{-1} [Fig. 4(*a*)]. The weak, sharp peaks at ≈6000 cm^{-1} are due to IR overtones, as may be seen from the reflectance spectrum of the analogous Zn^{II} compound [Fig. 4(*a*)]. The spectra recorded from a single crystal at 298 K and ≈12 K over the range 12 000–25 000 cm^{-1} are shown in Fig. 4(*b*). (The near-IR region was inaccessible due to the small size of the crystals.) The single broad peak which is centred at ≈16 300 cm^{-1} at 298 K is clearly resolved into bands at ≈16 800 and ≈14 600 cm^{-1} at ≈12 K [Fig. 4(*b*)].

The large energy separation between the bands in the electronic spectrum of $[Cu\{(C_5H_4N)_3CH\}_2][NO_3]_2$ is incompatible with a complex having six identical Cu–N bond lengths and a near octahedral geometry. Such a stereochemistry is expected to produce a single broad band centred at ≈13 000 cm^{-1}, as is observed for the first electronic transition of the corresponding Ni^{II} complex. On the contrary, the observed spectrum of $[Cu\{(C_5H_4N)_3CH\}_2][NO_3]_2$ is closely similar to those of $[Cu\{(pz)_2(C_5H_4N)CH\}_2][NO_3]_2$ and $[Cu\{(pz)_3CH\}_2][NO_3]_2$. The Cu^{II} atoms in both these compounds have tetragonally elongated octahedral geometries, with Cu–N bond distances similar to those deduced from the EXAFS of $[Cu\{(C_5H_4N)_3CH\}_2][NO_3]_2$.

EPR Spectra.—At 293 K the EPR spectrum of powdered $[Cu\{(C_5H_4N)_3CH\}_2][NO_3]_2$ is characteristic of an isotropic *g* value. On cooling to 150 K, although the *average g* value remains unchanged, the spectrum largely changes to that expected for a complex with a tetragonally elongated octahedral geometry (Fig. 5). This behaviour is similar to that reported for the $[Cu(H_2O)_6]^{2+}$ ion in Cu^{2+}-doped $[Zn(H_2O)_6]SiF_6$,[22] and subsequently observed for several pure Cu^{2+} compounds.[23] It may be explained by assuming that each Cu^{2+} complex has a tetragonally elongated octahedral geometry, and that the long bonds are randomly distributed along the three metal–ligand bond directions. The different orientations are energetically equivalent, except for the small effects of 'strains' due to lattice defects, so that upon input of energy the direction of tetragonal elongation may switch from one bond to another. At low temperature, this switching is relatively slow and the EPR spectrum is anisotropic, as though it originated from the powder of a tetragonally elongated complex with the direction of the long axis of each complex fixed in space. At room

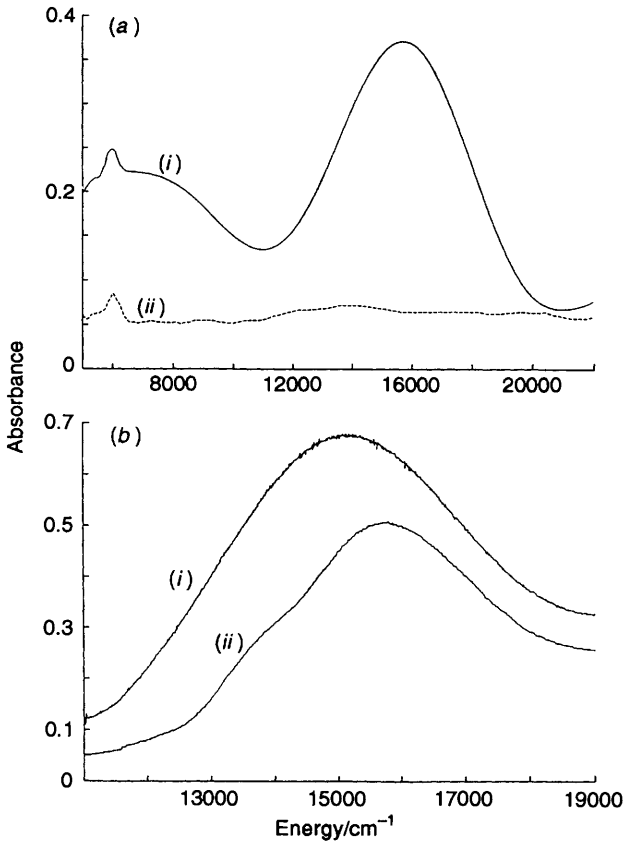

Fig. 4 (*a*) Room-temperature reflectance spectra of $[M\{(C_5H_4N)_3CH\}_2][NO_3]_2$, where M = Cu (*i*) and Zn (*ii*). (*b*) Electronic absorbance spectra (unpolarised light) from an arbitrary face of a crystal of $[Cu\{(C_5H_4N)_3CH\}_2][NO_3]_2$ at 298 K (*i*) and ≈12 K (*ii*)

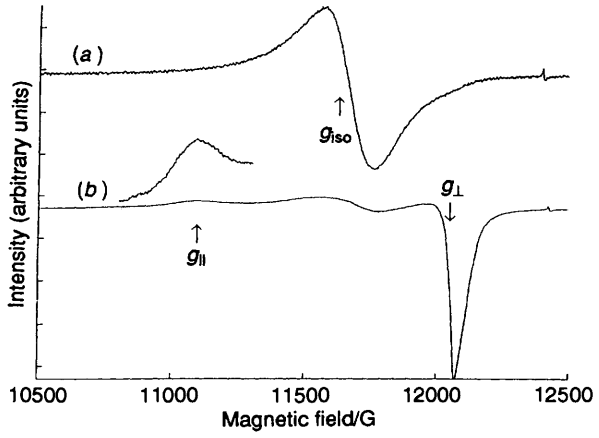

Fig. 5 The EPR spectrum of powdered $[Cu\{(C_5H_4N)_3CH\}_2][NO_3]_2$ measured at 293 K (*a*) and 150 K (*b*). The signal in the region of $g_\parallel$ at 150 K is also shown at an enhanced intensity. The weak inflections at a field of ≈12 400 G are due to a speck of powdered diphenylpicrylhydrazyl used as an internal standard (g = 2.0036)

temperature, the rate of switching is fast compared with the EPR time-scale, so that an isotropic signal is observed.

Two further aspects of the low-temperature EPR spectrum should be noted. First, a weak residual isotropic signal persists at low temperature (Fig. 5). This signal may originate from the fact that the random strains which act to localise the vibronic wave functions have a range of values, so that the rates at which the Cu–N bond lengths switch direction are not identical for all sites in the crystal. A similar behaviour has been observed in other systems of this type.[24] Secondly, the observation of a predominantly anisotropic signal at low temperature shows that the rate of *inter*molecular electron exchange in this compound is relatively slow. If the electron-exchange rate were fast enough to produce 'exchange narrowing', the random orientation of the bond axes would lead to the observation of an isotropic signal even at low temperature.

The EPR spectrum thus confirms that at the local level $[Cu\{(C_5H_4N)_3CH\}_2][NO_3]_2$ has a tetragonally elongated octahedral geometry. The g values derived from the low-temperature spectrum ($g_\parallel$ = 2.244, $g_\perp$ = 2.067) are characteristic of a ground state with the unpaired electron in the $d_{x^2-y^2}$ orbital, consistent with the complex having a tetragonally elongated octahedral geometry, as confirmed conclusively by the EXAFS. The g values are similar to those reported for the tetragonally elongated complexes formed by Cu^{2+} with analogous tripod ligands.[6,7] In the following section we show that similar values ($g_\parallel$ = 2.252, $g_\perp$ = 2.059) are also obtained by CAMMAG calculations using an isotropic orbital reduction parameter k = 0.78.

Metal–Ligand Bonding in Terms of the Angular Overlap Model.—A convenient method of parametrising the energy levels of transition-metal complexes is provided by the angular overlap model (AOM). This approach has recently been used to analyse the electronic spectra of complexes with a variety of tripod ligands.[6,7] It is of interest to see whether the transition energies of $[Cu\{(C_5H_4N)_3CH\}_2][NO_3]_2$ may be interpreted using chemically reasonable bonding parameters.

Calculations were carried out using the computer program CAMMAG developed by Gerloch and co-workers.[25] This program estimates the transition energies using a set of bonding parameters e_σ, $e_{\pi x}$, $e_{\pi y}$ to define the σ- and π-bonding characteristics of each ligand. The geometry is derived from an appropriate crystal structure. For the purposes of the calculations, the geometry of the present complex was assumed to be similar to that of $[Cu\{(pz)_2(C_5H_4N)CH\}_2][NO_3]_2$.[6] The crystallographically determined Cu–N distances in the latter complex are close to those determined for the present complex by the EXAFS analysis described above. An effective spin–orbit coupling constant of 645 cm^{-1} was used. π-Bonding in the plane of the amine ligand, represented by $e_{\pi x}$, was assumed to be negligible ($e_{\pi x}$ = 0), as found in other studies.[7] When the values used for the other bonding parameters were e_σ = 5800 cm^{-1}, $e_{\pi y}$ = 900 cm^{-1} for the four equatorial ligands, and e_σ = 2300 cm^{-1}, $e_{\pi y}$ = 350 cm^{-1} for the two axial ligands, the calculated transition energies were in reasonable agreement with those observed experimentally (see below).

Calc.: 17 350, 16 000, 14 600, 7050 cm^{-1}
Obs.: 16 800, ≈14 600, ≈7000 cm^{-1}

The bonding parameters of the closer (equatorial) nitrogen atoms are similar to those derived for other complexes with metal–ligand bond lengths comparable to the value 2.04 Å determined from the EXAFS of $[Cu\{(C_5H_4N)_3CH\}_2][NO_3]_2$.[6,7] For example, in $[Cu\{(pz)_2(C_5H_4N)CH\}_2][NO_3]_2$, e_σ = 6590 cm^{-1}, $e_{\pi y}$ = 1300 cm^{-1} for two N(pyridyl) atoms at 2.020 Å, and e_σ = 5540 cm^{-1}, $e_{\pi y}$ = 740 cm^{-1} for two N(pyrazolyl) atoms at 1.994 Å.[6]

On the other hand, if the bonding parameter e_σ varies as the inverse of the fifth or sixth power of the bond distance, as suggested by other studies,[6,7,26] then the value predicted for the Cu–N distance of 2.25 Å determined from the EXAFS study is $e_\sigma \approx 3000$ cm^{-1}. The value obtained for the axial ligands in $[Cu\{(C_5H_4N)_3CH\}_2][NO_3]_2$ is significantly lower, e_σ = 2300 cm^{-1}. A deviation of this kind is in fact always observed for Cu^{2+} complexes with a tetragonally elongated octahedral geometry, being generally explained in terms of configuration interaction between the $a_{1g}(z^2)$ and metal $a_{1g}(4s)$ orbitals.[27] The present discrepancy corresponds to a depression of ≈1400 cm^{-1} in the energy of the $^2A_{1g}(z^2)$ excited state, which is very similar to that deduced for an axial bond length of 2.3 Å in a

study of a series of tetragonally distorted Cu^{II} amine complexes by Deeth and Gerloch.[28] Even smaller values, e_σ = 800 and 500 cm^{-1}, were obtained for the bonding parameters of the axial ligands in the complexes $[Cu\{(pz)_2(C_5H_4N)CH\}_2][NO_3]_2$ and $[Cu\{(pz)_3CH\}_2][NO_3]_2$, respectively.[6,7] The depression in e_σ is expected to increase as the tetragonal distortion increases. For the Cu^{2+} complexes of the above three tripod ligands, the decrease in the e_σ values of the axial ligands, 2300 > 800 > 500 cm^{-1}, does indeed mirror the increase in the axial bond lengths, 2.3 < 2.355 < 2.385 Å. Thus the AOM calculations are consistent with the relatively short axial bond length derived from the EXAFS analysis of $[Cu\{(C_5H_4N)_3CH\}_2][NO_3]_2$.

Conclusion

The results illustrate the differences between the information provided by the various techniques. X-Ray diffraction reveals atomic positions averaged over the lattice as a whole. In $[Cu\{(C_5H_4N)_3CH\}_2][NO_3]_2$ the ligand atoms of the tetragonally elongated $[Cu\{(C_5H_4N)_3CH\}_2]^{2+}$ complex are disordered to give a space-averaged geometry with six identical Cu–N bond lengths. It is not clear why the disorder is not apparent in the vibrational ellipsoid parameters produced by the X-ray analysis, but the *absence* of a significant asymmetry in such parameters cannot be taken as evidence that the atoms are localised at the observed positions. In contrast, the electronic spectrum and EXAFS are determined by the true local ligand geometry about each Cu^{2+}. Provided that, as in the present case, intermolecular electron exchange is slow, EPR spectroscopy lies between these two extremes. An isotropic spectrum is observed at room temperature where the ligand atoms interchange position rapidly, but at 150 K the signal becomes anisotropic because the ligand exchange rate has dropped below the EPR timescale.

Acknowledgements

The X-ray absorption data were recorded at the Australian National Beamline Facility (ANBF) at the KEK Photon Factory, Tsukuba, Japan. The research was supported by grants A29131459 (to M. A. H.), AL9132720 (to E. R. T. T.), A28415896 (to F. R. K.) and A29230677 (to H. C. F. and J. M. Guss) from the Australian Research Council, and by a travel grant from ANBF. P. J. E. was the holder of an Australian Postgraduate Research Award.

References

1 S. Trofimenco, *Chem. Rev.*, 1972, **72**, 497; *Prog. Inorg. Chem.*, 1986, **34**, 115.
2 T. A. Hafeli and F. R. Keene, *Aust. J. Chem.*, 1988, **41**, 1379.
3 P. S. Moritz, A. A. Diamantis, F. R. Keene, M. R. Snow and E. R. T. Tiekink, *Aust. J. Chem.*, 1988, **41**, 1352.
4 F. R. Keene, M. R. Snow, P. J. Stephenson and E. R. T. Tiekink, *Inorg. Chem.*, 1988, **27**, 2040.
5 P. A. Anderson, F. R. Keene, E. Horn and E. R. T. Tiekink, *Appl. Organomet. Chem.*, 1990, **4**, 523.
6 T. Astley, A. J. Canty, M. A. Hitchman, G. L. Rowbottom, B. W. Skelton and A. H. White, *J. Chem. Soc., Dalton Trans.*, 1991, 1981.
7 T. Astley, J. M. Gulbis, M. A. Hitchman and E. R. T. Tiekink, *J. Chem. Soc., Dalton Trans.*, 1993, 509.
8 D. L. Cullen and E. C. Lingafelder, *Inorg. Chem.*, 1970, **9**, 1858.
9 D. Tucker, P. S. White, K. L. Trojan, M. L. Kirk and W. E. Hatfield, *Inorg. Chem.*, 1991, **30**, 823.
10 P. J. Ellis, H. C. Freeman, M. A. Hitchman, D. Reinen and B. Wagner, *Inorg. Chem.*, 1994, **33**, 1249.
11 M. A. Hitchman, *Transition Met. Chem. (New York)*, 1985, **9**, 1.
12 N. Walker and D. Stuart, *Acta Crystallogr., Sect. A*, 1983, **39**, 158.
13 TEXSAN, Single Crystal Structure Analysis Software, Version 1.6, The Woodlands, Molecular Structure Corporation, TX, 1993.
14 C. K. Johnson, ORTEP II, ORNL Report 5136, Oak Ridge National Laboratory, TN, 1976.
15 P. J. Ellis, unpublished work.
16 J. J. Rehr and R. C. Albers, *Phys. Rev. B*, 1990, **41**, 8139; J. J. Rehr, J. Mustre de Leon, S. I. Zabinsky and R. C. Albers, *J. Am. Chem. Soc.*, 1991, **113**, 5135; J. Mustre de Leon, J. J. Rehr, S. I. Zabinsky and R. C. Albers, *Phys. Rev. B*, 1991, **44**, 4146.
17 M. A. Hitchman, *Comments Inorg. Chem.*, 1994, **15**, 197.
18 N. W. Isaacs and C. H. L. Kennard, *J. Chem. Soc. A*, 1969, 386; M. D. Joesten, M. S. Hussain, P. G. Lenhert and J. H. Veneble jun., *J. Am. Chem. Soc.*, 1968, **90**, 5623; M. D. Joesten, M. S. Hussain and P. G. Lenhert, *Inorg. Chem.*, 1970, **9**, 151.
19 D. L. Cullen and E. C. Lingafelder, *Inorg. Chem.*, 1971, **10**, 1264; J. H. Ammeter, H. B. Bürgi, E. Gamp, V. Sandrin-Meyer and W. P. Jensen, *Inorg. Chem.*, 1979, **18**, 733.
20 J. S. Wood, C. P. Keijzers, E. de Boer and A. Buttafava, *Inorg. Chem.*, 1980, **19**, 2213; M. Stebler and H. B. Bürgi, *J. Am. Chem. Soc.*, 1987, **109**, 1395.
21 P. Chaudhuri, K. Oder, K. Wieghardt, J. Weiss, J. Reedijk, W. Hinrichs, J. Wood, A. Ozarowski, H. Stratemeier and D. Reinen, *Inorg. Chem.*, 1986, **25**, 2951.
22 B. Bleaney and D. J. E. Ingram, *Proc. Phys. Soc., Ser. A*, 1950, **63**, 408.
23 D. Reinen and S. Krause, *Solid State Commun.*, 1979, **29**, 691; R. C. Koch, M. D. Joesten and J. H. Venable, *J. Chem. Phys.*, 1973, **59**, 6312.
24 M. J. Riley, M. A. Hitchman, D. Reinen and G. Steffen, *Inorg. Chem.*, 1988, **27**, 1924.
25 D. A. Cruse, J. E. Davies, M. Gerloch, J. H. Harding, D. Mackey and R. F. McMeeking, CAMMAG, a Fortran Computing Package, University of Cambridge, 1979.
26 M. Bermejo and L. Pueyo, *J. Chem. Phys.*, 1983, **78**, 854.
27 L. G. Vanquickenborne and A. Ceulemans, *Inorg. Chem.*, 1981, **20**, 796.
28 R. Deeth and M. Gerloch, *Inorg. Chem.*, 1984, **23**, 3849.

Received 16*th September* 1994; *Paper* 4/05652C